JJEES

JJEES (2025) 16 (1): 67-74
ISSN 1995-6681

Jordan Journal of Earth and Environmental Sciences

Modeling Recharge Rates of Stormwater Ponds into the Vadose Zone: A Case Study in a Semi-Arid Region

Tamer Eshtawi*

Department of Engineering and Smart Systems, University College of Applied Sciences, P.O. Box 1415, Palestine

Received on 28 May 2024, Accepted on 30 December 2024

Abstract

In this study, the basic soil hydrologic processes within the vadose zone were simulated using the Hydrus-2D/3D package, which presented a numerical solution to Richards equation (derived from Darcy's law). The flow through the vadose zone was modeled for five cases of moderate periods of infiltration (≤ 10 days), as practiced in stormwater harvesting ponds in the Gaza Strip. The five cases comprise: (a) three cases of surface infiltration, including three sizes of infiltration ponds, namely 25 × 25 m, 50 × 50 m, and 100 × 100 m and (b) two cases of dry well infiltration, with two sizes of infiltration ponds, namely 25 × 25 m having 9 dry wells, and 50 × 50 m, having 49 dry wells. For the surface infiltration cases, Darcy's gradient fit equation was determined to be (i = 2.4 − 0.24 ln (Pond Area, A)). In the case of dry wells, the infiltration capacity decreased from 93 m³/day to 90.9 m³/day using 9 dry wells and further declined to 81.7 m³/day with 49 dry wells. Results reveal that infiltration rates decrease over time, with surface infiltration showing a notable reduction due to groundwater mounding, especially in larger ponds. Despite lower initial rates, dry well infiltration maintains greater stability and reduced mounding impact, suggesting its suitability for sustained recharge in semi-arid areas. The general empty dry well equation can be modified by a factor of 0.25 to 0.3 for large infiltration ponds to fit the case of a dry well filled with gravel. The study provides insight into the dynamic interactions between pond size, infiltration method, and groundwater mounding, highlighting essential design considerations.

© 2025 Jordan Journal of Earth and Environmental Sciences. All rights reserved

Keywords: *Vadose zone; Infiltration rate; Stormwater harvesting; Dry wells infiltration, Hydrus 2D/3D*

1. Introduction

Recharge could be classified according to the source (De Vries and Simmers, 2002). Natural recharge is related to precipitation that infiltrates beneath the ground. In contrast, artificial recharge is a process of replenishing groundwater by the percolated surface water into the aquifer layer through various methods depending on the topographic, geologic, and groundwater conditions. The vadose zone influences the hydrologic cycle, which includes two major components of the water budget: surface runoff and percolation (Dillon, 2002). Quantifying water recharge in the vadose zone is still a research topic, especially in the context of urban water resources (He et al., 2024). There are different techniques, that could be utilized to estimate the infiltration rate into the vadose zone, e.g., Darcy's flux method, Green-Ampt models, and Richards' equation models. The Richards' equation, known for its detailed representation of unsaturated flow through porous media, is often regarded as the most accurate approach for modeling infiltration rates (Hsu et al., 2002). The Green-Ampt model, although simpler and less computationally demanding, has shown comparable performance to the Richards' equation in many practical cases (Williams et al., 1998).

Surface infiltration through ponds is a common recharge technique requiring permeable soil layers as well as an unconfined aquifer, whereas sufficient lateral flow is required to reduce groundwater mounding impact. Thus, a hydrogeological assessment is required to do the first screening and to select the proper sites. Where suitable geological layers, as well as suitable land areas for surface infiltration, are not available, vertical infiltration systems should be raised as a proper solution, such as dry wells in the vadose zone. Vadose zone wells are carried out using a bucket auger, and they could be about 0.6 – 1.2 m in diameter and reach 80 m deep. Clogging of the infiltration surface is a debatable problem that could result in a dramatic reduction of the infiltration rate into the topsoil and vadose zone (Bouwer, 2002).

Despite the simplicity of Darcy's law for one-dimensional saturated flow (Darcy, 1856), which is a function of the saturated hydraulic conductivity and the hydraulic gradient. The hydraulic gradient reflects the potential flow forces (e.g., gravity and capillary suction) causing water to infiltrate beneath the recharge facility. The variation of the hydraulic gradient is a function of the time of the infiltration event, the geology of the infiltration layers, and the groundwater depth. For a very short period of potential infiltration (e.g., less than a day for sandy soil), the initial infiltration is greater than the saturated hydraulic conductivity (K_s) since the hydraulic gradient value is greater than 1.0. Whereas infiltration will be around the (K_s) values for longer periods, then decrease to less than the (K_s) values as the wetting front (Green-Ampt concept) reaches the water table (Massmann et al., 2003).

* Corresponding author e-mail: teshtawi@ucas.edu.ps

In light of the above, some research has been carried out to estimate the hydraulic gradient under these circumstances using imperial methods. For example, Drost et al. (1999) performed different computer simulations to derive the effective gradient empirical formula under steady-state conditions for surface infiltration as well as infiltration trenches. However, there is a need for research depicting the unsteady state behavior of the infiltration process, including the change of the hydraulic gradient, especially for cases of short to medium infiltration periods, e.g., storm events in a semi-arid area.

The Richards' equation is a very common partial differential equation to simulate the vertical flow in the vadose zone, taking into account the variation of the hydraulic gradient (Zha et al., 2019). In spite of the applicability of the analytical solution, the numerical solution is recommended for its flexibility in dealing with boundary and initial conditions (Pachepsky et al., 2003).

Using finite element software is a significant approach to modeling the unsteady-state infiltration rate, considering the Richards' equation. The Hydrus software is a physical/numerical-based model, utilizing a finite-element method to simulate the movement of water as well as multiple solutes in different saturated media. Simunek and Weihermüller (2018) used Hydrus-1D to investigate the impact of soil, the initial water content of soil, and potential boundary conditions on the infiltration rate. Farasati and Shakeri (2018) used Hydrus-1D to infer the hydraulic parameters to model water infiltration rates in loamy soil for four pre-identified locations, considering the reverse method. Ying et al. (2020) utilized the Hydrus-1D to investigate a modified Green-Ampt model to quantify infiltration through a column of 3.0 m and five soil layers. Rasheed and Sasikumar (2015) used neural networks and white numerical models based on system knowledge to simulate the unsaturated flow process, taking feed-forward neural network architecture into account. With a recent update of Hydrus modeling techniques, Sasidharan et al. (2020) compared the efficiency of the dry wells as well as the surface infiltration basins under similar conditions using the Hydrus (2D/3D) software.

In the Gaza Strip, a semi-arid region, there are several ponds for stormwater infiltration as well as treated wastewater recharge; however, some of these ponds failed to meet the estimated infiltration rates. Several issues could be raised as reasons for system failure, including design criteria or equations and clogging during operation. Infiltration via dry wells, which are filled with gravel (0.6 - 0.8 m borehole diameter), has been used in Gaza to overcome the existence of shallow impermeable soil layers that can dramatically reduce a pond's infiltration rate. However, there are a lot of debates about the effectiveness of this alternative. Additionally, the chemical composition of groundwater depends on the recharge rate from anthropogenic sources, such as stormwater ponds, which can disrupt fragile groundwater systems either by polluting them or altering the hydrological cycle (Onwuka et al., 2010; Okogbue and Ukpai, 2013). The investigation of different infiltration systems and the simulation of their infiltration rates using a comprehensive technique can support future infiltration facilities as well as solve efficiency problems in similar current ponds. In this study, the vertical infiltration through the soil layers was addressed by Richards' equation to simulate the basic soil hydrologic processes in the vadose zone.

Not only does the study reflect the modeling of surface infiltration rate scenarios, but it also simulates the overall transient infiltration capacity of different sets of dry wells during discrete storm events in Gaza.

The study aims to simulate the infiltration rates of two main recharge techniques practiced in Gaza, namely surface infiltration and dry wells, taking into account soil hydraulic conductivity and groundwater level. The objectives of this study are to carry out (1) a 3D modeling of surface infiltration rates for different cases or combinations of pond areas and (2) a 3D modeling of dry well infiltration rates for a different combination of pond areas reflected in different numbers of dry wells. The study demonstrates a temporal simulation of the infiltration rates with different systems and sizes to be used as a guide for the proper design of stormwater infiltration facilities.

2. Study Area and Existing Recharge Facilities

The Gaza Strip is located in the eastern part of the Mediterranean; its climate is characterized as that of a semi-arid region. In Gaza, around 2.2 million people live within an area of 365 km^2, according to 2021 statistics (PCBs, 2021). Stormwater harvesting is considered a crucial policy that should be continuously embraced by the Palestinian Authority and implemented in different large projects, e.g., roads, industrial estates, etc. Large-scale infiltration facilities were taken into account over the last 10 years as a major non-conventional water resource in Palestine, particularly in the Gaza Strip (Hamdan et al., 2007). Gaza has faced continuous depletion of its underground resources due to withdrawals exceeding the total recharge of the aquifer. Consequently, the stored volume continues to decrease, similar to other semi-arid regions like Jordan, making efficient groundwater recharge essential (Bentahar et al., 2023). No specific location in Gaza was used in this study; however, the average period of storm events, the average groundwater elevation for most of the harvesting ponds, and soil hydraulic parameters are the main characteristics of the study area reflected in the model parameters.

2.1 Topography

The land surface topography of the Gaza Strip ranges from 0 (near the sea) to around 108 meters of elevation. Figure 1 (a) exhibits the digital elevation model of the Gaza Strip with a raster resolution of 30 m (USGS, 2021).

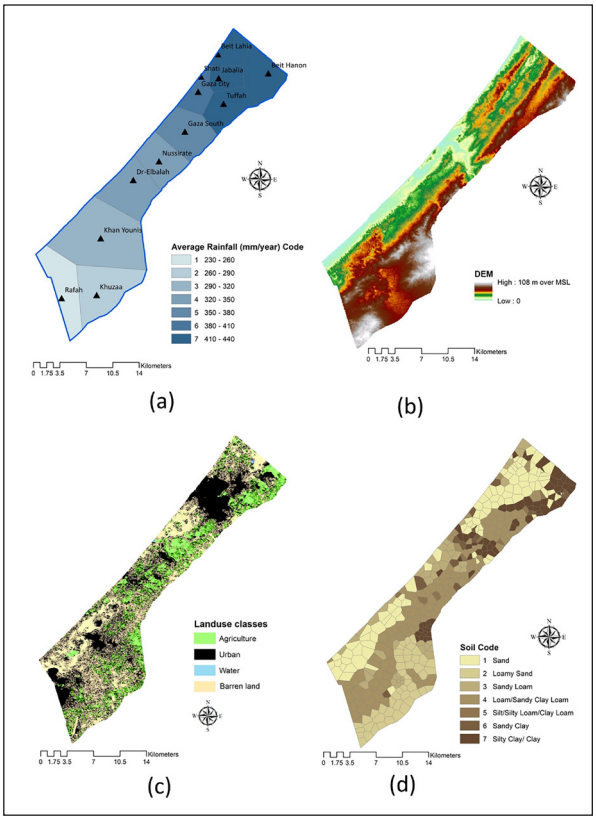

Figure 1. Gaza Strip: (**a**) Rainfall distribution (MoA, 2021); (**b**) Topography; (**c**) Landuse (developed by the author for year-2023; (**d**) Soil (MoA, 2021)

2.2 Climate

The climate of the study area varies, taking rainfall into account; the average annual rainfall for the Gaza strip is around 315 mm (around 415 mm for the north and 225 mm for the south). The annual pan evaporation is about 1620 mm in Gaza City (MOA, 2021), and the mean temperature varies between 14 °C in January and 28 °C in August (MOA, 2021). Rainfall is the main source of replenishment for the Gaza coastal aquifer. In the Gaza Strip, there are 12 daily rainfall stations distributed among the five Gaza governorates. Figure 1 (b) shows the average annual rainfall quantities of the 12 rainfall stations for the period 1976–2021. The daily rainfall data depicts that continuous storm events could, at their maximum before a significant stop, range between 5 and 10 days, which is a crucial factor in stormwater pond design in terms of hydraulic gradient calculation.

2.3 Soil and landuse

Three dominant land-use classes can be depicted in the Gaza Strip, namely, agricultural land, barren land, and urbanized areas representing more than 20 % of the Gaza Strip area (Figure 1 (c). Figure 1(d) depicts a soil map of the Gaza Strip, classified into seven soil textures according to the percentage of sand, silt, and clay. The main composition of the coastal soil (sand dunes) of the Gaza Strip is quartz and alumina silicate. Its layer thickness ranges from 2 m to about 50 m and extends up to 4 to 5 km, especially in the northern and southern areas. Sandy loess soils, loessial sandy soils, and loess soils prevail in the southeast part of the Strip. The soil in the north and east of Gaza is richer in silt, clay, and loess. Loess soil represents the main soil class around the valleys with a thickness of around 25 to 30 m (MoA, 2021).

2.4 Vadose Zone Characteristics

The vadose zone is the unsaturated zone above the groundwater level that represents the space between the topsoil and the water table. The vadose zone is functionally similar to that of aquifer media in terms of its permeability. The vadose zone media within the study area is classified as sandstone layer (50%), sand and sandstone (30%), and clay and sandstone (20%) (Al-Hallaq and Elaish, 2012). According to different experimental and technical studies, the saturated vertical hydraulic conductivity ranges from 2 to 6 m/day (4 m/day on average) for the sandstone layers that could be suitable for infiltration techniques. Under the stormwater ponds, the typical geological characteristics depict different formations of sandy layers and sandy loam layers that are suitable for infiltration as well as clay, silty clay, or sandy silty clay layers that have very low permeability. In some cases, the low permeable soil is shallow, which raises the need for a dry well technique to penetrate this layer to a more suitable one for infiltration. The groundwater depth beneath the majority of the stormwater infiltration ponds ranges between 15 and 25 meters.

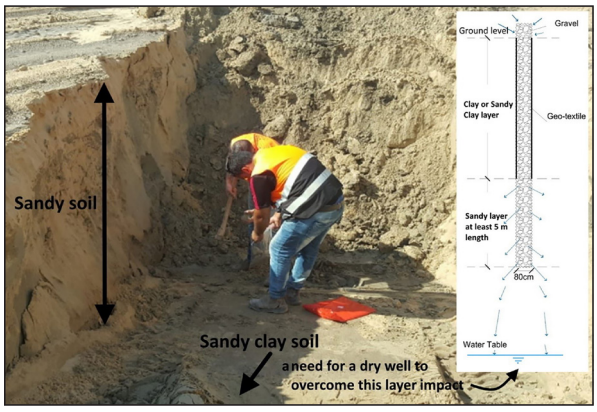

Figure 2. A real photo taken during the excavation for a stormwater pond depicting the need for dry well technique to penetrate a low permeable layer

Figure 2 shows a real photo taken during the excavation to construct a stormwater pond. The first 2 m were sandy soil, followed by a sand clay layer (very low permeable soil) with a thickness ranging from 8 m to 12 m before reaching a sandstone layer (sandy soil) with a saturated hydraulic conductivity of 4 m/day.

3. Vadose zone flow modeling

Vadose zone flow for five infiltration cases was modeled using the Hydrus-2D/3D package. The Hydrus, including its additional modules, solves the Richards' equation, using numerical techniques for saturated and unsaturated water flow and convection-dispersion type equations for heat and solute transport (Yu and Zheng, 2010).

Considering Richards' equation as the governing equation for the targeted model, Darcy's law for one-dimensional saturated flow is the basis for this equation, which can be expressed as equation (1).

$$q = K_s i = -K_s \frac{dH}{dl} \quad (1)$$

where K_s is the saturated hydraulic conductivity, H is the hydraulic pressure head, and (i) or dl/dl is the hydraulic gradient (defined as the change in total head per the unit length of the flow pathway). However, for unsaturated conditions, the hydraulic conductivity is a function of moisture content θ (it ranges between 0 and 1), so Darcy's law for unsaturated media (in one dimension) can be depicted as in equation (2).

$$q = -K(\theta)\frac{dH}{dl} \quad (2)$$

when the hydraulic pressure head (H) is a function of h (the capillary pressure head, which is a function of the moisture content θ) and z (the elevation head), then, Darcy's law can be written as in equation (3).

$$q = -K(\theta)\frac{d(h(\theta)+z)}{dz} \quad (3)$$

Given this relationship $\partial\theta/\partial t = -\partial q/\partial z$, the mass-conservative form of the Richards equation for 3D flow can be written as follows in equation (4) (Gasiorowski and Kolerski, 2020):

$$\frac{\partial\theta}{\partial t} = \frac{\partial}{\partial z}\left(K_z(h)\frac{\partial h}{\partial z} - K_z(h)\right) + \frac{\partial}{\partial x}\left(K_x(h)\frac{\partial h}{\partial x}\right) + \frac{\partial}{\partial y}\left(K_y(h)\frac{\partial h}{\partial y}\right) \quad (4)$$

where θ (h) represents volumetric water content; h refers to the pressure head (unsaturated zone has negative pressure), t is time; x, y, and z represent spatial variables, (m), and $K_x(h)$, $K_y(h)$, and $K_z(h)$ are unsaturated hydraulic conductivity in the mentioned spatial variables, (m/s).

The vadose zone hydraulic properties (e.g., soil water retention parameters) could be depicted by Mualem–van Genuchten (MVG) formulas (Simunek et al., 2006); however, this study utilized Modified Mualem–van Genuchten that improves the hydraulic conductivity characterization near saturation to get a converged solution (Schaap and Genuchten, 2005), especially regarding dry-wells cases. In the transient simulation process, the minimum time step was 0.001 days (1.44 min), which is a very important parameter; Hydrus could diverge with larger values when there was a sudden change in boundary fluxes.

3.1 Surface infiltration cases

Three cases of surface infiltration were simulated, taking into account three sizes of infiltration ponds, namely 25 × 25 m, 50 × 50 m, and 100 × 100 m. The water table is estimated to be approximately 20 meters below the soil surface (an average value among different stormwater ponds in Gaza). The soil water pressure head, an initial condition, was defined to be a constant pressure head of 0.5 m for the infiltration domain as depicted in Figure 3. The model domain for different cases was discretized into a three-dimensional triangular finite element mesh utilizing the MESHGEN tool under the umbrella of Hydrus, as tabulated in Table 1. The mesh was refined at the bottom of the infiltration area where a large water flux was expected. The depth of the overall domain was 30 m for all cases. The saturated hydraulic conductivity was 4 m/day.

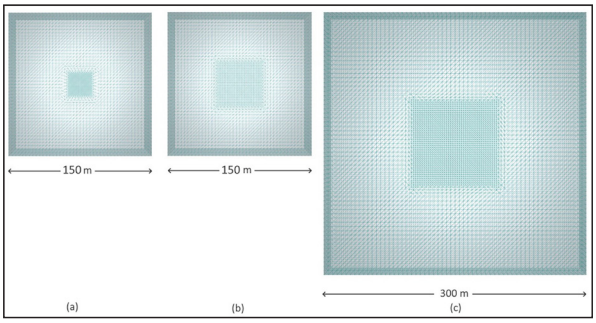

Figure 3. Finite element meshes (top plan) for the surface infiltration cases: (**a**) the modeling domain of 150 × 150 m and 25 × 25 m top infiltration domain; (**b**) the modeling domain of 150 × 150 m and 50 × 50 m top infiltration domain; (**c**) the modeling domain of 300 × 300 m and 100 × 100 m top infiltration domain.

3.2 Dry well infiltration cases

Two cases of dry well infiltration were simulated, taking into account two sizes of infiltration ponds namely, 25 × 25 m comprising 9 dry wells, and 50 × 50 m comprising 49 dry wells. The dry wells have a diameter of 0.8 m and were filled with gravel. The distance between the bottom of the dry well and the water table is 5 m for the two dry well cases. The soil moisture was considered to be uniform throughout the infiltration zone, whereas the capillary fringe was considered to be below the bottom of the dry well, and the soil domain surrounding the dry well installation was considered an unsaturated zone.

Table 1. Numerical model characteristics (surface infiltration)

Case	Characteristics
(a)	Total Domain: 150 × 150 × 30 m, 114,186 3D-elements Mesh size: 3.6 m (large), 0.9 m (small) Constant head: 0.5 m Infiltration space: 25 × 25 m Ks: 4 m/day GW depth: –20 m
(b)	Total Domain: 150 × 150 × 30 m, 104,691 3D-elements Mesh size: 3.6m (large), 1.8m (small) Constant head: 0.5 m Infiltration space: 50 × 50m Ks: 4 m/day GW depth: –20 m
(c)	Total Domain: 300 × 300 × 30 m, 162,906 3D-elements Mesh size: 5 m (large), 2.5 m (small) Constant head: 0.5 m Infiltration space: 150 × 150 m Ks: 4 m/day GW depth: –20 m

The soil water pressure head, an initial condition, was defined to be a constant pressure head of 0.5 m for the infiltration domain as depicted in Figure 4. The simulation domain was discretized into a three-dimensional triangular finite element mesh using the MESHGEN tool available within the Hydrus (2D/3D) as tabulated in Table 2. The mesh was refined at the bottom of the infiltration area where a large water flux was expected. The depth of the overall domain was 32 m for all cases. The saturated hydraulic conductivity was estimated for the infiltration sandstone layer (after a 10-m clay layer) to be 4 m/day. A top 2-meter sandy layer was

added as a natural filter to improve stormwater quality (as implemented in previous existing projects) with a saturated hydraulic conductivity of 8 m/day, making the water table 22 meters below the top of the added sand (or 20 meters, not considering this added layer).

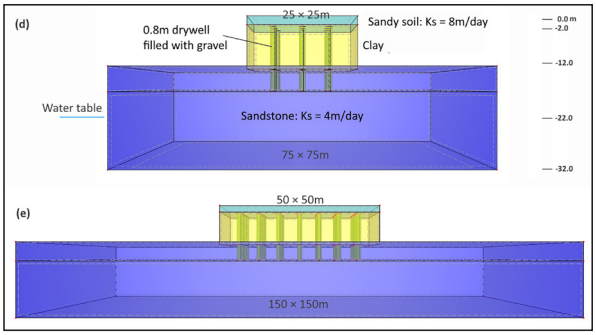

Figure 4. Finite element meshes for the drywells infiltration cases: (**d**) 9 dry wells; (**e**) 25 dry wells.

Table 2. Numerical model characteristics (dry wells)

Case	Characteristics
(d)	Total Domain: 173,612 3D-elements Mesh size: 2.4 m (soil layers), 0.8 m (dry wells) Constant head: 0.5 m Infiltration space: 25 × 25 m, 9 (diam. 80cm) Geological layers: 2 m top sand, 10 m clay, 5 m sandy layer, water table, 15 m sandy layer K_s for infiltration layer: 4 m/day K_s for top sandy layer: 8 m/day GW depth: –22 m
(e)	Total Domain: 185,739 3D-elements Mesh size: 5.0 m (soil layers), 0.8 m (dry wells) Constant head: 0.5 m Infiltration space: 50 × 50 m, 49 (diam. 80cm) Geological layers: 2 m top sand, 10 m clay, 5 m sandy layer, water table, 15 m sandy layer K_s for infiltration layer: 4 m/day K_s for top sandy layer: 8 m/day GW depth: –22 m

4. Results and Discussion

Modeling of recharge beneath stormwater ponds shows how the wetting front reaches the water table in terms of velocity as well as flux. The results illustrate a spatial-temporal behavior of infiltration taking into account two infiltration techniques, namely surface infiltration and dry well infiltration. The results show that there are negative relationships between the infiltration rate and the area of infiltration, as well as between the infiltration rate and the time of infiltration. The simulation results are depicted in Figures 5 to 10. The figures show the Darcy's velocities as well as the infiltration rates (from the output mass balance information) after 1 day, 5 days, and 10 days of simulation.

Regarding the surface infiltration cases, the infiltration rate obviously decreased from 4.1 m/day (case a) to 3.5 m/day (case c which has a higher infiltration area) on day 1, and similarly from 3.5 m/day to 0.9 m/day on day 10. The impact of groundwater mounding that occurs beneath stormwater ponds is obvious in case (c) exhibiting a dramatic decrease in the infiltration rate (from 3.5 m/day to 0.9 m/day). This impact is clear in the lag in colored contours of Darcy's velocity with time from day 1 to day 10 (decreased from 4 m/day to around zero in the middle of the pond for case (c)).

After 10 days of the simulation, a pond area of 625 m^2 (case a) lost around 15% of its initial infiltration rate. Similarly, cases (b) (pond area 2,500 m^2) and (c) (pond area 10,000 m^2) show losses of their initial infiltration capacities of around 47% and 74%, respectively. Referring to Darcy's equation (Equation 1) (the hydraulic gradient (i) was simulated to be 0.88, 0.51, and 0.23 for cases (a), (b), and (c), respectively.

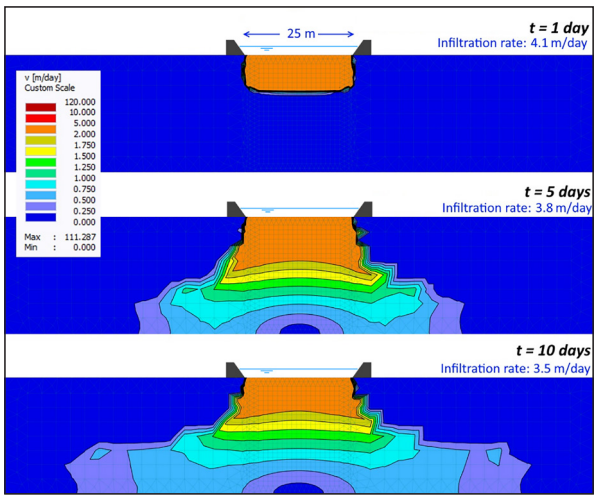

Figure 5. Darcy's velocity and infiltration rate in the vadose zone (20 m) (Case a).

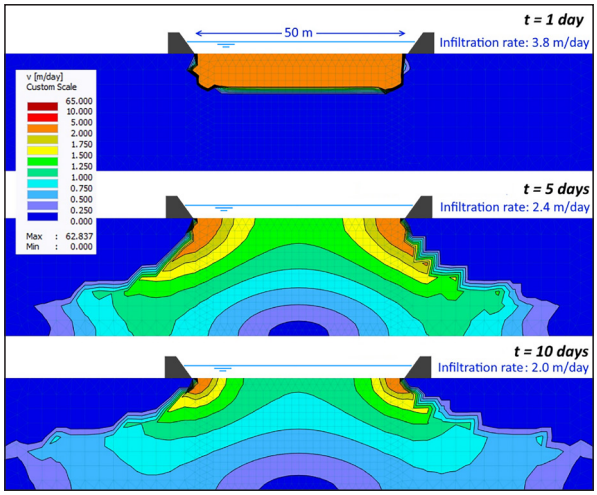

Figure 6. Darcy's velocity and infiltration rate in the vadose zone (20 m) (Case b).

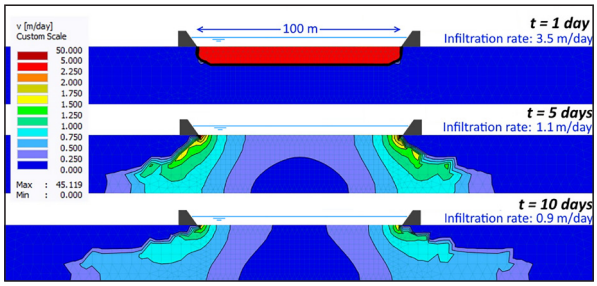

Figure 7. Darcy's velocity and infiltration rate in the vadose zone (20 m) (Case c).

Figure 8 depicts the relationships between the stormwater pond area (A) (> 500 m^2) and the gradient (*i*) for the three surface infiltration cases. Taking into account that a 10-day infiltration rate is suitable for the rainfall pattern in the

Gaza Strip, equation 5 is a deduced equation to estimate the Darcy gradient for general cases of stormwater ponds in the Gaza Strip as well as in other semi-arid regions with similar groundwater levels.

$$i = 0.24(10.1 - \ln(A)) \quad (5)$$

A comparison between the hydraulic gradient results obtained and those obtained using the empirical formula proposed by Massmann et al., 2003 is illustrated in Figure 8. Massmann equation is a steady state equation (Equation 6), to estimate hydraulic gradient (i) considering water depth in the pond (D_{pond}) (m), water table depth (D_{wt}) (m), infiltration area (A) (m^2), and saturated hydraulic conductivity (K_s) (m/s). It provides more conservative hydraulic gradient results because it deals with a steady-state situation rather than short to moderate infiltration periods (≤ 10 days).

$$i = 8.46 \times \frac{D_{wt}+D_{pond}}{K_s^{0.1}} A^{-0.76} \quad (6)\ \text{(Massmann et al., 2003)}$$

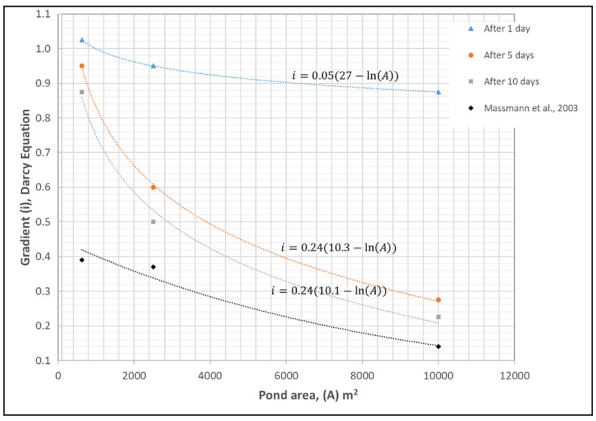

Figure 8. The relationship between the stormwater pond area (A) and the gradient (i) for the three surface infiltration cases

For the dry wells' infiltration cases, Figures 9 and 10 illustrate Darcy's velocity and the infiltration capacity for a dry well. The infiltration rates for the two cases were slightly lower compared with the surface infiltration cases, reflecting the lower impact of groundwater mounding. The dry well infiltration capacity decreased from 93 m^3/day to 90.9 m^3/day for case (d) and to 81.7 m^3/day for case (e) due to the grouping impact (multiple dry wells in one infiltration pond). The slight impact of groundwater mounding is clear in Case (e) on day 10, where the Darcy's velocity in some areas was reduced. Taking into account the dry well equation for empty boreholes (Equation 7) (not filled with gravels) (Bouwer, 2002):

$$Q = K_s 2\pi L_w^2 / \left\{ ln\left[\frac{L_w}{r_w} + \sqrt{\left(\frac{L_w^2}{r_w^2} - 1\right)}\right] - 1 \right\} \quad (7)$$

where Q is the infiltration rate (L^3/t), K_s represents the saturated hydraulic conductivity value (L/t), L_w refers to the length of the infiltration portion of the borehole (L), and r_w is the radius of the borehole (L). Figure 11 depicts these parameters.

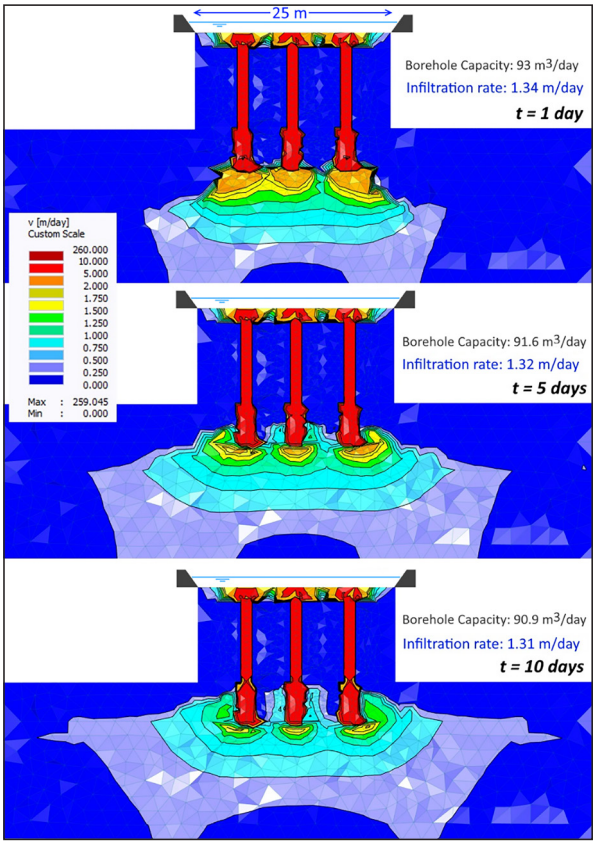

Figure 9. Darcy's velocity and infiltration rate (Case d)

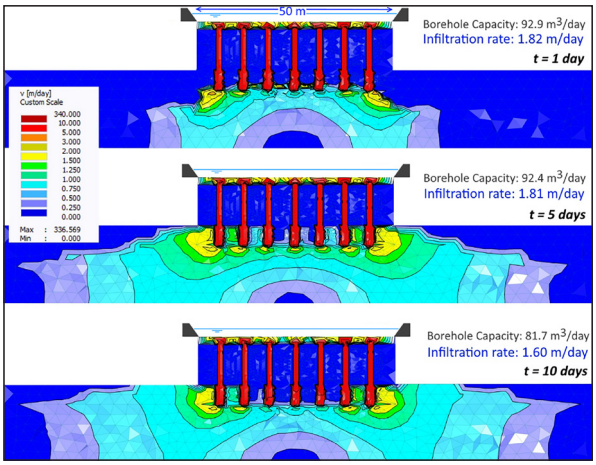

Figure 10. Darcy's velocity and infiltration rate (Case e)

The estimated Q for one borehole in the two-dry well cases was 283.2 m^3/day, not considering the grouping efficiency of the boreholes. This research result promotes a factor of around 0.3 (The model results, considering a gravel-filled dry well, show a value of 81.7, which is divided by the estimation from Equation 7 for an empty dry well = "81.7 / 283.2 = 0.3") to be used for modifying the dry well equation to fit the situation as well as the practice in Gaza (dry wells filled with gravel). This factor was deduced for a pond area of around 2,500 m^2 (around 50 m^2 for each dry well). According to the slight differences between the resulting values, this factor could be valid for larger ponds; however, it could be reduced to 0.25 for relatively larger ponds.

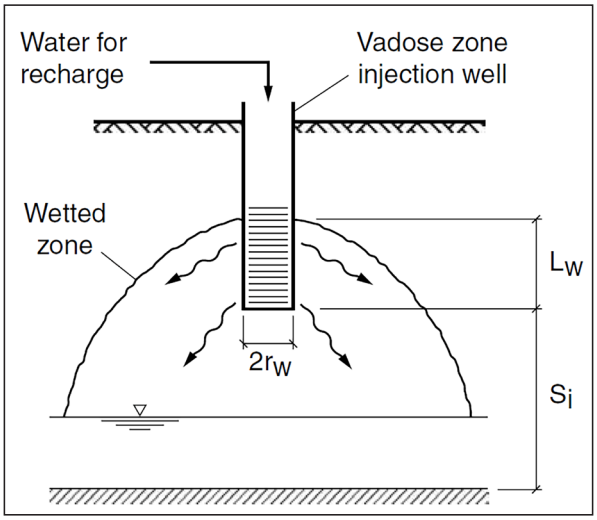

Figure 11. Dry wells parameters

The results of this study provide significant insights into the behavior of infiltration beneath stormwater ponds using both surface and dry well infiltration methods. The decreasing infiltration rates, observed over time, reflect the natural processes of soil saturation and groundwater mounding. In particular, the rapid decline in infiltration capacity for larger pond areas (e.g., case (c)) highlights the critical influence of pond size on groundwater recharge dynamics. This trend aligns with previous studies (e.g., Massmann et al., 2003), which indicate that larger infiltration areas result in lower hydraulic gradients, thereby reducing infiltration efficiency over time.

The comparison of surface and dry well infiltration also offers valuable practical insights. While the dry well method exhibited lower infiltration rates than surface methods, the reduced impact of groundwater mounding suggests its suitability for semi-arid regions, like Gaza, where maximizing infiltration over extended periods is crucial for groundwater recharge. Furthermore, the application of the Bouwer (2002) equation (Equation 7) for dry wells, combined with the deduced modification factor (0.3), provides a practical adjustment for engineers and hydrologists working in areas with similar geohydrological conditions. This factor allows for more accurate predictions of dry well performance, particularly when filled with gravel, as commonly practiced in Gaza.

However, there are several broader implications of these findings. The relationship between pond area and infiltration efficiency suggests that optimizing pond size for specific rainfall patterns and groundwater levels could enhance stormwater management strategies in semi-arid regions. This optimization could be particularly relevant for areas facing water scarcity, as more efficient infiltration designs could increase the recharge rate of local aquifers.

5. Conclusion and Recommendation

Hydrus-2D/3D was employed to estimate the infiltration rate into the vadose zone using two infiltration techniques, namely surface infiltration and dry well infiltration. Groundwater mounding, related to the infiltration pond area, has an obvious impact on reducing the infiltration rate for the surface infiltration technique.

The surface infiltration for a moderate infiltration period (10 days) was around 0.9 m/day for a pond area (A in m^2) of 10,000 m^2, which could be estimated as . Whereas, for the dry well technique, around 82 m^3/day is the capacity for one borehole after 10 days of infiltration. The hydraulic gradient (i) was estimated to be around 0.23 for large infiltration ponds on the 10^{th} day of the simulation. This value can be used for large infiltration ponds (around 10,000 m^2) utilized for stormwater harvesting purposes (10 days of infiltration simulates two storm events in a semi-arid region like Gaza). Equation 3, used for flow estimation through a dry well, can be modified by a factor of 0.25 to 0.3 for large infiltration ponds to fit the case of a dry well filled with gravel (a vertical trench). This factor comprises the impact of constructing several dry wells in one pond, and the time of infiltration. Extending the research cases to include a longer simulation time as well as a larger infiltration pond area to cover the infiltration of continuous effluent from treated wastewater is recommended. Although Massmann et al. (2003) equation (Equation 6) reflects a slight change in the hydraulic gradient (i) due to any significant change in the saturated hydraulic conductivity (in the equation, K_s was raised to a small power ($K_s^{0.1}$)), investigating the sensitivity of saturated hydraulic conductivity and its impact on the hydraulic gradient will be useful in supporting more design practices for infiltration techniques in Gaza.

From another side, the Massmann equation provides a conservative estimate of hydraulic gradients under steady-state conditions, the differences observed between the empirical and model results suggest that more research is needed to adapt these general equations to the short- to medium-term infiltration periods typical in stormwater management practices. Future work could also focus on refining the modified Bouwer equation for dry wells to better account for variations in pond size and groundwater levels, as well as other influencing factors such as soil heterogeneity and compaction.

Moreover, the sensitivity of the infiltration rates to groundwater mounding raises questions about long-term sustainability. While the model results provide a 10-day snapshot, longer-term simulations are necessary to assess how continued stormwater recharge might impact groundwater quality, particularly in areas with high contamination risk. Studies on the transport of pollutants during infiltration events (especially in urban areas) could help determine the suitability of these methods for both quantity and quality management of groundwater.

Finally, this research demonstrates the concept of effective blue-green infrastructure that depicts natural systems and artificial facilities covering urban water systems (blue infrastructure, e.g., stormwater harvesting ponds, and green infrastructure, e.g., natural habitats, ecosystems, and urban greenspace).

Acknowledgments

This research was supported by MEDRC Water Research Innovation Initiative Award – Palestine.

Conflict of Interest

The author declares that he has no known competing financial interests or personal relationships that could have appeared to influence the work reported in this paper.

References

Al-Hallaq, A., and Elaish, B. (2012). Assessment of aquifer vulnerability to contamination in Khanyounis Governorate, Gaza Strip—Palestine, using the DRASTIC model within GIS environment. Arabian Journal of Geosciences, 5: 833–847.

Bentahar, F., Mesbah, M., and Ribstein, P. (2023). Hydrogeological modeling of the sandstone aquifer of Mostaganem Plateau (North-West Algerian) and perspectives on the evolution of withdrawals. Jordan Journal of Earth and Environmental Sciences, 14(2): 113-125.

Bouwer, H. (2002). Artificial recharge of groundwater: Hydrogeology and engineering. Hydrogeology Journal, 10(1): 121–142.

Dillon, P.J. (Ed.) (2002). Management of aquifer recharge for sustainability: Proceedings of the 4th International Symposium on Artificial Recharge of Groundwater (ISAR-4), Adelaide, South Australia, 22–26 September 2002. A.A. Balkema Publishers, Lisse, Netherlands, 561p.

De Vries, J.J., and Simmers, I. (2002). Groundwater recharge: An overview of processes and challenges. Hydrogeology Journal, 10: 5-17.

Farasati, M., and Shakeri, H. (2018). Simulation of water infiltration in the soil using HYDRUS-1D software and field data. Journal of Water and Soil Conservation, 25(3): 113-128.

Gasiorowski, D., and Kolerski, T. (2020). Numerical solution of the two-dimensional Richards equation using alternate splitting methods for dimensional decomposition. Water, 12: 1780.

Hamdan, S.M., Troeger, U., and Nassar, A. (2007). Stormwater availability in the Gaza Strip, Palestine. International Journal of Environment and Health, 1(4): 580.

He, Y., Wang, Y., Liu, Y., Peng, B., and Wang, G. (2024). Focus on the nonlinear infiltration process in deep vadose zone. Earth-Science Reviews, 252: 104719.

Hsu, S.M., Ni, C.F., and Hung, P.F. (2002). Assessment of three infiltration formulas based on model fitting on Richards equation. Journal of Hydrologic Engineering, 7(5): 363-374.

Massmann, J. (2003). Implementation of infiltration pond research. Washington State Transportation Commission Department of Transportation in cooperation with U.S. Department of Transportation Federal Highway Administration. WA-RD 578.1.

MoA (Ministry of Agriculture) – Palestine. (2021). Archived data.

Okogbue, C.O., and Ukpai, S.N. (2013). Geochemical evaluation of groundwater quality in Abakaliki area, southeast Nigeria. Jordan Journal of Earth and Environmental Sciences, 5(1): 1-8.

Onwuka, S.O., Ezeh, C.S., and Ekwe, A.C. (2010). Application of chemometric technique in the assessment of groundwater quality in Udi and its environs, South-eastern Nigeria. Jordan Journal of Earth and Environmental Sciences, 3(2): 63-78.

Pachepsky, Y., Timlin, D., and Rawls, W. (2003). Generalized Richards' equation to simulate water transport in unsaturated soils. Journal of Hydrology, 272(1-4): 3-13.

PCBS (Palestinian Central Bureau of Statistics). (2021). Palestinians at the end of year 2017. Ramallah–Palestine. Retrieved from http://www.pcbs.gov.ps.

Rasheed, S., and Sasikumar, K. (2015). Modeling vertical infiltration in an unsaturated porous media using neural network architecture. Aquatic Procedia, 4: 1008-1015.

Sasidharan, S., Bradford, S., Simunek, J., and Kraemer, S. (2020). Comparison of recharge from dry wells and infiltration basins: A modeling study. Journal of Hydrology, 594(4): 125720.

Schaap, M.G., and Van Genuchten, M.T. (2006). A modified Mualem-van Genuchten formulation. Vadose Zone Journal, 5: 27–34.

Simunek, J., Van Genuchten, M.T., and Sejna, M. (2006). The HYDRUS software package for simulating two- and three-dimensional movement of water, heat, and multiple solutes in variably-saturated media. Technical manual. Version 1.0. Prague: PC Progress, 241p.

Simunek, J., and Weihermüller, L. (2018). Using HYDRUS-1D to simulate infiltration. Retrieved from https://www.pc-progress.com.

USGS (US Geological Survey). (2022). EarthExplorer [Online]. Available from: http://earthexplorer.usgs.gov.

Williams, J.R., Ying, O., Chen, J.S., and Ravi, V. (1998). Estimation of infiltration rate in the vadose zone: Application of selected mathematical models. Volume 2.

Ying, M., Shaoyuan, F., Dongyuan, S., Guangyao, G., and Zailin, H. (2010). Modeling water infiltration in a large layered soil column with a modified Green–Ampt model and HYDRUS-1D. Computers and Electronics in Agriculture, 71(1): 40-47.

Yu, C., and Zheng, C. (2010). HYDRUS: Software for flow and transport modeling in variably saturated media. Software Spotlight, Groundwater, 48(6): 787-791.

Zha, Y., Yang, J., Zeng, J., Tso, C.H.M., Zeng, W., and Shi, L. (2019). Review of numerical solution of Richardson–Richards equation for variably saturated flow in soils. WIREs Water. First published: 19.